International Journal of Heat and Mass Transfer 51 (2008) 5671–5678

Contents lists available at ScienceDirect

International Journal of Heat and Mass Transfer

journal homepage: www.elsevier.com/locate/ijhmt

Computerized planning of cryosurgery using bubble packing: An experimental validation on a phantom material

Michael R. Rossi [a], Daigo Tanaka [b,1], Kenji Shimada [a,b], Yoed Rabin [a,*]

[a] Department of Mechanical Engineering, Carnegie Mellon University, 5000 Forbes Avenue, Pittsburgh, PA 15213, United States
[b] Department of Biomedical Engineering, Carnegie Mellon University, 5000 Forbes Avenue, Pittsburgh, PA 15213, United States

ARTICLE INFO

Article history:
Received 2 November 2007
Received in revised form 4 April 2008
Available online 18 June 2008

Keywords:
Cryosurgery
Prostate
Planning
Experimental validation
Bioheat transfer simulation
Bubble packing

ABSTRACT

The current study focuses on experimentally validating a planning scheme based on the so-called bubble-packing method. This study is a part of an ongoing effort to develop computerized planning tools for cryosurgery, where bubble packing has been previously developed as a means to find an initial, uniform distribution of cryoprobes within a given domain; the so-called force-field analogy was then used to move cryoprobes to their optimum layout. However, due to the high quality of the cryoprobe distribution suggested by bubble packing and its low computational cost, it has been argued that a planning scheme based solely on bubble packing may be more clinically relevant. To test this argument, an experimental validation is performed on a simulated cross-section of the prostate, using gelatin solution as a phantom material, proprietary liquid nitrogen-based cryoprobes, and a cryoheater to simulate urethral warming. Experimental results are compared with numerically simulated temperature histories resulting from planning. Results indicate an average disagreement of 0.8 mm in identifying the freezing front location, which is an acceptable level of uncertainty in the context of prostate cryosurgery imaging.

1. Introduction

Cryosurgery is the destruction of undesired biological tissues by freezing [1]. Modern cryosurgery is frequently performed as a minimally-invasive procedure, with the application of multiple cooling probes (cryoprobes), in the shape of long hypodermic needles, strategically located in the area to be destroyed (the target region) [2].

While there is an extensive body of literature on the factors affecting cryosurgery success [3], it is the match between the frozen region contour and the outer surface of the target region which is currently used for cryosurgery control. This match is evaluated with the application of an imaging device such as MRI, but more commonly with ultrasound [4–7]. The cryoprobe layout is a key factor for achieving the highest correlation between the frozen region and the target region and, therefore, for the success of cryosurgery. While crystal formation at the freezing front is known to be the cornerstone of cryoinjury, it continues to progress over a wide temperature range, with a lower boundary commonly known as the "lethal temperature" threshold (−45 °C is possibly the most commonly accepted value for the lethal temperature [3]).

To date, cryoprobe localization is an art held by the cryosurgeon, based on the surgeon's own experience and accepted practices. Suboptimal cryoprobe localization may leave areas in the target region untreated, lead to cryoinjury of healthy surrounding tissues, require an unnecessarily large number of cryoprobes, increase the duration of the surgical procedure, and increase the likelihood of post cryosurgery complications; all of which affect the quality and cost of the medical treatment. Computerized planning tools would help to alleviate these difficulties, which is the subject matter of this ongoing research program at the Biothermal Technology Laboratory [8–16].

The difficulties associated with planning a minimally-invasive cryoprocedure have been widely acknowledged by other researchers, and efforts to develop computerized means to facilitate planning are reported in the literature [17–19]. The focus at the Biothermal Technology Laboratory has been to develop more efficient planning tools which could be utilized in practice. Towards that goal, the so-called force-field analogy technique has been developed, which executes a series of heat transfer simulations and automatically relocates cryoprobes between consecutive runs until an optimum cryoprobe layout is found [8,9]. In addition, an algorithm termed "bubble packing" has been implemented to predict the best initial condition for the force-field analogy procedure, in order to decrease the number of iterations required in the optimization process [15]. Although originally designed solely for generating the initial cryoprobe configuration for planning, the high

* Corresponding author. Tel./fax: +1 412 268 2204.
E-mail address: rabin@cmu.edu (Y. Rabin).
[1] Present address: WesternGeco – Schlumberger, Research and Engineering, 10001 Richmond Avenue, Houston, TX 77042, United States.

0017-9310/$ - see front matter © 2008 Elsevier Ltd. All rights reserved.
doi:10.1016/j.ijheatmasstransfer.2008.04.045

quality of the cryoprobe distribution resulting from bubble packing has made the need for further optimization via the force-field analogy debatable [14]. Even though the force-field analogy offers superior results, the improvement is typically minor and is accompanied by a dramatically longer planning run time.

The objective of the current study is to experimentally validate a computerized planning scheme based solely on bubble packing. For this purpose, an experimental apparatus for 2D cryosurgery simulation has been recently developed, along with a technique for analysis of the frozen region shape based on video recording [11]. In the current study, experimental results are used to define a set of target region shapes. Next, the planning scheme is executed and its quality is evaluated by how well bubble packing predicts the actual experimental cryoprobe locations. The quality of bubble packing is further discussed in the context of the resulting temperature field and freezing front location. Although the current experimental validation is performed in 2D—for technical reasons—the bubble-packing method has already been extended and demonstrated in 3D [16].

2. Experimental setup

The experimental system has been presented elsewhere [11] and is presented here in brief only, for the completeness of presentation. With reference to Fig. 1, the experimental system is designed for 2D cryosurgery simulation on a gelatin solution as a phantom material, where the 2D setup is representative of a prostate cross-section. The thermophysical properties of pure water are in close range to those of soft biological tissues [10]; gelatin (1.6% by weight) is added to the water to prevent convective heat transfer in the domain. In order to accentuate the contrast between the frozen and unfrozen regions, blue food dye is added to the gelatin solution. The gelatin container is made of 5 mm-thick Plexiglas plates, with a gelatin chamber of 25 mm × 200 mm × 200 mm.

Proprietary liquid-nitrogen based cryoprobes [11] are used in the current study. These are similar in principle to the original cryoprobes invented by Cooper and Lee in 1961 [1], with the exception of an off-center internal feeding tube, and an embedded T-type thermocouple in the outer wall to record temperature data. The cryoprobes are made of copper, having an external diameter of 3.2 mm. Up to six cryoprobes are used concurrently, with an average cooling rate of 33 °C/min in the first three minutes of operation, and a minimum operation temperature of nearly −110 °C at the outer wall when approaching steady state.

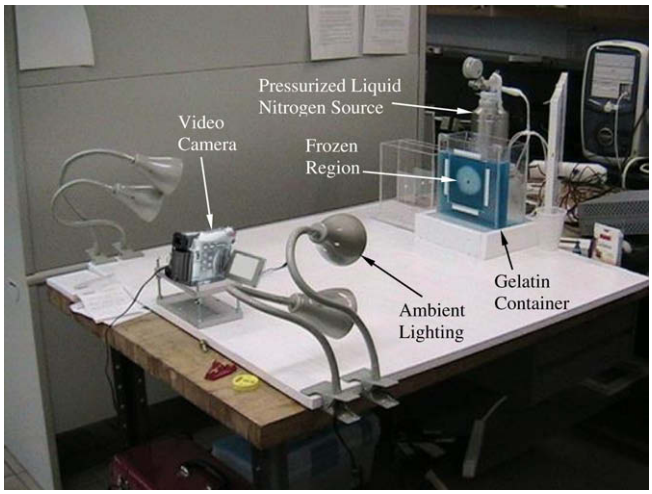

Fig. 1. The experimental setup.

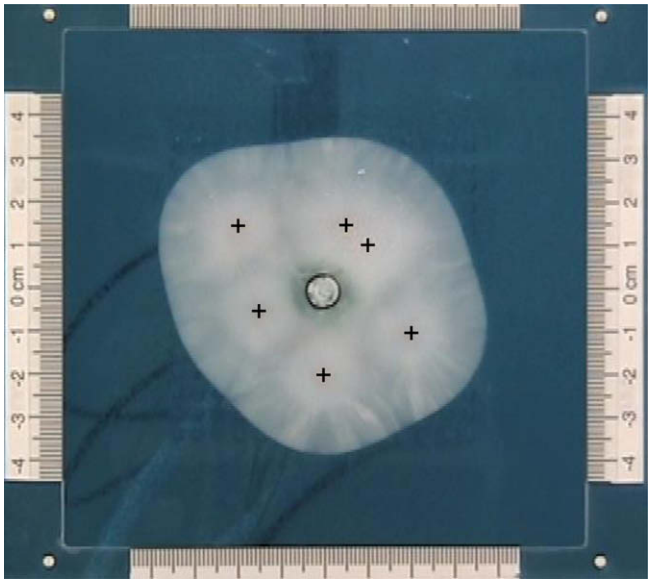

Fig. 2. The frozen region as recorded by the camcorder (layout E in Fig. 4); the cryoprobe locations are additionally marked with plus signs.

Urethral warming in the current setup is simulated by means of a cryoheater [10,20]. The cryoheater used in the current study is a 90 Ω electric cartridge heater, which is placed inside a 7 mm O.D. thin-wall brass tube. A temperature controller is used to maintain the temperature of the cryoheater at a constant 25 °C throughout the experiment; this temperature level was chosen, because it does not affect the integrity of the gelatin links, whereas 37 °C would ideally be used for urethral warming in a clinical operation. The cryoheater, along with the cryoprobes, are inserted through appropriately sized holes in the back of the gelatin chamber.

Experiments are video-recorded in the current study, using the Canon ZR300 Mini DV camcorder, as shown in Fig. 1. A typical view from the camcorder is shown in Fig. 2, where four measuring scales are placed at the perimeter of the field of view on the wall of the gelatin chamber. Additionally, four white dots are marked at the corners of the field of view for registration purposes.

3. Computational methods

3.1. Geometric modeling: frozen region reconstruction

The frozen region reconstruction technique has been presented recently [11], and is reviewed here in brief only, for completeness of presentation. For the purpose of frozen region reconstruction, each movie of a freezing experiment is converted into a sequence of snapshots (Fig. 2), which are then converted into grayscale images, while using the Matlab "unsharp" filter to sharpen the freezing front. Next, a region-growing segmentation technique is applied, starting from seed points located at the centers of the imaged cryoprobes (represented by "+" in Fig. 2). Pixels are then systematically added to the frozen domain, based on their level of intensity and proximity to previously added pixels. Finally, upon completion of the segmentation, a dilation transformation is performed to enlarge the segmented region in order to fill small holes and gaps in the imaged frozen region. By comparison with manual segmentation, the uncertainty in this automated technique is estimated as 2% of the frozen region size [11], which corresponds to an average of 0.25 mm uncertainty in identification of the freezing front location.

3.2. Planning algorithm: bubble packing

Bubble packing is a physically based approach to search for an even distribution of a selected number of objects inside a given geometrical domain [21]. The bubble packing scheme generates spherical elements (or bubbles) inside the domain first, the centers of which are the points to be distributed. The boundary of the domain is described by a different set of bubbles, which are stationary and have infinitesimal volume (i.e., boundary bubbles). Next, van der Waals-like forces are simulated to move the non-stationary bubbles, until a minimum-force configuration is found. Generally, the van der Waals model represents coupled attraction and repulsion forces between every two elements in the domain, where attraction forces become dominant at great distances, while repulsion forces become dominant at a short distance. It is the combined forces among all the bubbles in the domain that dictates their final relative location—known as the equilibrium layout. Once bubbles are defined (or seeded) in the domain, their forced motion is numerically simulated until equilibrium is reached.

Consistent with previous studies [14–16], the van der Waals model is simplified to:

$$f(l) = \begin{cases} \alpha l^3 + \beta l^2 + \gamma l + \varepsilon & 0 \leqslant l \leqslant 1.5 l_0 \\ 0 & 1.5 l_0 < l \end{cases} \tag{1}$$

subject to the following boundary conditions:

$$f(l_0) = f(1.5 l_0) = 0, \quad f'(0) = 0, \quad f'(l_0) = -\kappa_0 \tag{2}$$

where l is the distance between two interacting bubbles, l_0 is the equilibrium distance if only two isolated bubbles are interacting, κ_0 is the a linear spring constant at distance l_0, and α, β, γ, and ε are the coefficients of the simplified van der Waals forcing function.

In the current study, three major modifications are made to the previously developed bubble-packing method [14–16]: (i) eliminating attraction forces, which means that the negative-value region of Eq. (1) is being truncated; (ii) increasing the radius of boundary bubbles; and (iii) changing the amount by which adjacent bubbles are permitted to overlap (known as the overlap ratio). The overlap ratio between the ith bubble and its neighbors is defined as [15]:

$$\alpha_i = \frac{2}{d_i} \sum_{j=0}^{n} \left(d_i + \frac{d_j}{2} - \overline{x_i x_j} \right) \tag{3}$$

where index j represents a neighbor bubble, d is the diameter of the bubble, x is location, and n is the number of neighboring bubbles.

The above modifications yield higher quality cryoprobe layouts than the results from [14–16] for the particular geometries used in the current study. Furthermore, eliminating attraction forces accelerates computational time. However, it is noted that the quality of bubble packing in the current work is not evaluated merely by measuring the volumetric distribution of bubble centers, but rather by evaluating the transient temperature fields resulting from bioheat simulations. Hence, the above modifications must be viewed as specific improvements for cryosurgical applications, rather than general improvements for bubble packing. It is further noted that the modified bubble-packing method works only if boundary bubbles are defined, otherwise bubbles will always move away from one another.

As an example, the cryoprobe layout illustrated in Fig. 3a was obtained by the original bubble packing method, where some bubbles were attracted towards the center of the target region. The cryoprobe layout in Fig. 3b was obtained after eliminating attractive forces, resulting in bubbles distributed along the boundary of the domain. Finally, the effects of increasing the overlap ratio and increasing boundary bubble size are illustrated in Fig. 3c. From a trial-and-error study, a boundary bubble radius of 4 mm and an overlap ratio of 7.4 were found to be the best-fit parameters, where the quality of the bubble packing was evaluated by executing a bioheat transfer simulation for each layout, as discussed below. Compared with the original bubble packing scheme, the modified scheme yielded superior results in terms of matching the planned cryoprobe layout with the experimental cryoprobe locations.

3.3. Physical modeling: bioheat transfer simulation

Consistent with previous studies [8,9,13–15,22] the classical bioheat equation [23] is used to model heat transfer during prostate cryosurgery:

$$C \frac{\partial T}{\partial t} = \nabla \cdot (k \nabla T) + \dot{w}_b C_b (T_b - T) + \dot{q}_{met} \tag{4}$$

where C is the volumetric specific heat of the tissue, T is the temperature, t is the time, k is the thermal conductivity of the tissue, $\dot{w}_b$ is the blood perfusion volumetric flow rate per unit volume of tissue, C_b is the volumetric specific heat of the blood, T_b is the blood temperature entering the thermally treated area, and $\dot{q}_{met}$ is the metabolic heat generation. The domain examined in the current study is pure water and, therefore, the blood perfusion and metabolic heating effects are set to zero. Note that heating due to blood perfusion during cryosurgery is a second-order effect and metabolic heat generation is negligible [22]. The physical properties used for

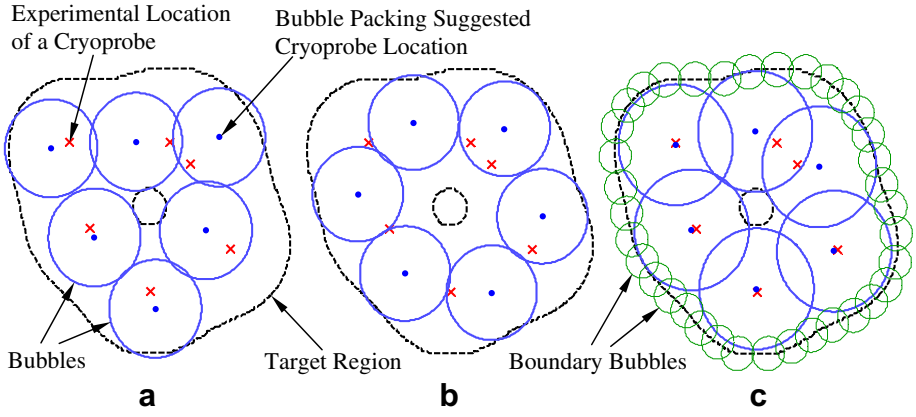

Fig. 3. The effect of algorithm modifications on the quality of bubble packing, demonstrated on Case 14: (a) results of the original scheme, (b) results after attractive forces are eliminated, and (c) results with a modified overlap ratio and an increased boundary bubbles radius.

Table 1
Thermophysical properties used in the current analysis (pure water), and typical thermophysical properties of biological tissues, where T is the temperature in degree K [9,10,26]

Property	Water		Biological tissues	
Thermal conductivity k (W/m K)	0.58	$273 < T$	0.50	$273 < T$
	$2135 \times T^{-1.235}$	$T < 273$	$16.0–0.0567 \times T$	$251 < T < 273$
			$1005 \times T^{-1.15}$	$T < 251$
Volumetric specific heat C (MJ/m^3 K)	4.20	$275 < T$	3.60	$273 < T$
	86.6	$271 < T < 275$	15.4	$251 < T < 273$
	$0.0078 \times T$	$T < 271$	$0.00398 \times T$	$T < 251$
Latent heat L (MJ/m^3)	333.7		300	
Blood perfusion heating effect w_b, C_b (kW/m^3 K)	0		0–40	

the current study are listed in Table 1, and for comparison purposes, the physical prosperities used to model biological tissues are also presented. Eq. (4) is solved using the finite difference numerical scheme presented in [22].

While water (as a pure material) freezes at a unique temperature, biological tissues freeze over a wide temperature range, typically −22 °C to 0 °C, if first-order approximated as an NaCl solution [22]. While the numerical technique is most suited to simulate phase-transition over such a temperature range—as the scheme is based on the enthalpy approach—special care must be taken in the current study, when simulating water as a pure material. In the current study, a pseudo phase-transition temperature range is assumed between −2 °C and +2 °C; it has been demonstrated that a pseudo phase-transition temperature range maintains the numerical scheme consistency with respect to the freezing front location, while introducing some uncertainty in the

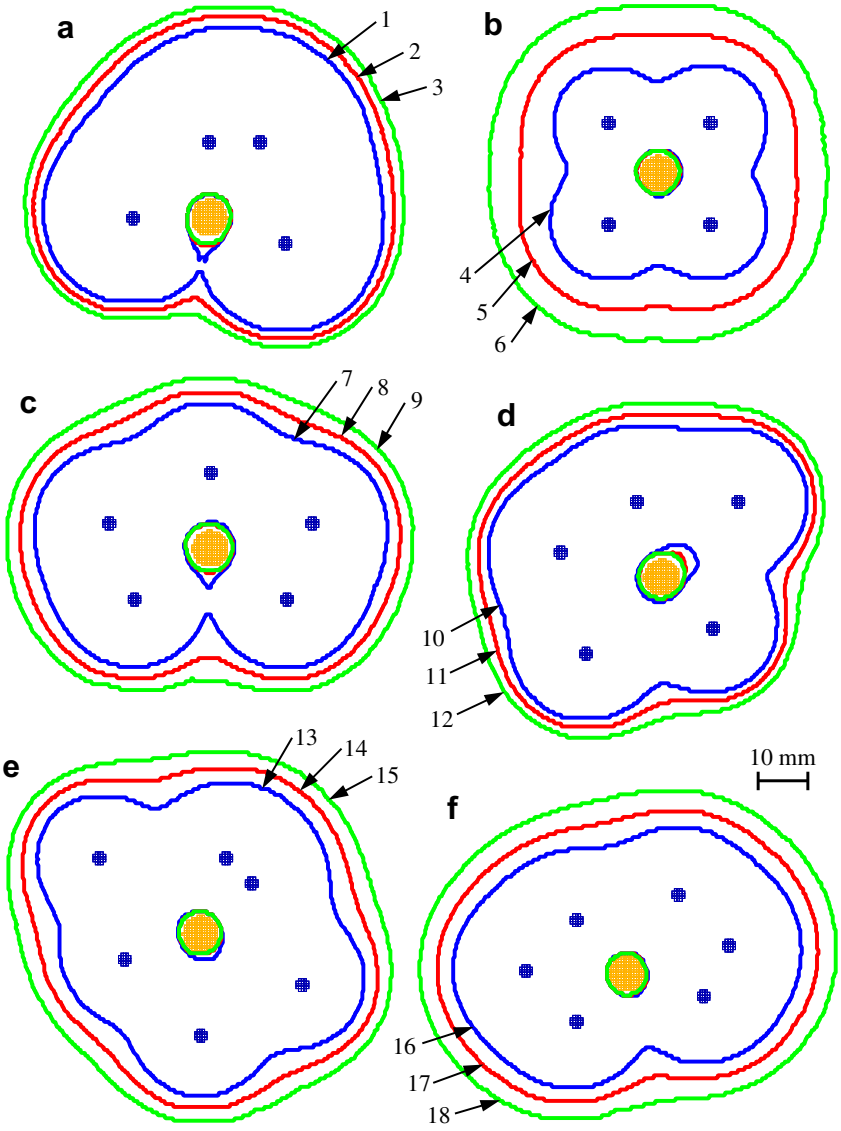

Fig. 4. Reconstructed freezing front from experiments using six cryoprobe layouts (a–e), each at three points in time, defining the target region shape for the 18 cases analyzed in the current study.

actual temperature distribution around it [24]. For comparison purposes with experimental data, the temperature isotherm of −2 °C has been selected to represent the freezing front in numerical simulations, since it is consistent with the enthalpy formulation as the point of phase transition completion.

3.4. Comparison criterion: the defect region concept

Once a target region is defined, the current planning tool is aimed at maximizing internal cryodestruction while minimizing its external effect. Thus, in the absence of more detailed clinical requirements, the objective for planning is to lower the temperature of the entire target region below a specific isotherm value determined by the surgeon, while keeping the temperature of the surrounding tissue above this value. For previous studies [8,9], the −22 °C isotherm was selected for demonstration purposes since it represents both the lower boundary of phase-transition in biological tissues and the mid-range temperature between the onset of freezing and the lethal temperature (between 0 °C and −45 °C). In the current study however, the biological tissue is simulated with a gelatin solution, for which the lower pseudo phase-transition boundary is −2 °C (see Section 3.3, above). Therefore, the overall defect in the current study is defined as:

$$G = \frac{1}{A_E}\int_{A_s} w\,dA_s; \quad w = \begin{cases} 1 & -2\ ^\circ C < T_s \quad \text{interior to the experimental frozen region} \\ 0 & T_s \leqslant -2\ ^\circ C \quad \text{interior to the experimental frozen region} \\ 1 & T_s \leqslant -2\ ^\circ C \quad \text{exterior to the experimental frozen region} \\ 0 & -2\ ^\circ C < T_s \quad \text{exterior to the experimental frozen region} \end{cases} \tag{5}$$

where A_s is the area of the simulated domain, A_E is the area of the reconstructed frozen region from video recordings, and w is a weight function, dependent on the simulated temperature field, T_s. A bioheat simulation is run until the time of minimum defect between experimental data and numerical results, and its minimum value is recorded for the purpose of analysis and discussion.

4. Results and discussion

Experimental results for six different cryoprobe layouts are reported in this study. From each experiment, three different points in time were selected, representing different stages in the evolution of the frozen region; each such point in time represents one target region for planning, yielding a total of 18 target regions for investigation. Fig. 4 displays reconstruction results for all 18 cases, while Table 2 lists the corresponding numerical data. Note that Case 14 in Fig. 4 displays segmentation results for the snapshot presented in Fig. 2.

Bioheat transfer simulations were performed under the following conditions: a standard domain area of 130 mm × 130 mm [11]; a uniform grid size of 0.5 mm [12]; a constant urethral warmer temperature of 25 °C; all cryoprobes follow the same cooling protocol, starting at 0 °C and linearly cooling down to −110 °C within 30 s, and held constant thereafter.

From Table 2, it can be seen that the defect value for bubble packing results, D_{bp}, ranges from 3.9% to 8.0%, with an average value 6.1%. The defect value for heat transfer simulation based on the actual experimental cryoprobe locations, D_{exp}, ranges from 1.9% to 5.8%, with an average value of 3.3%. For any given case, D_{exp} is smaller than D_{bp}, where the value of D_{exp} is associated with the quality of the heat transfer simulation itself, while the difference between D_{exp} and D_{bp} is attributed to the quality of planning.

The average difference between the simulated freezing front at the end of bubble packing and the segmented freezing front, ΔS_{bp}, is also listed in Table 2. The average difference is calculated by dividing the absolute defect area by the perimeter of the target re-

Table 2
Summary of results: n is the number of cryoprobes; t_{exp} is the time at which the target region is reconstructed from video recording; A_{exp} is the reconstructed area of the target region

No.	Lay-out	n	t_{exp} (min)	A_{exp}, mm^2	D_{bp} (%)	D_{exp} (%)	t_{bp} (min)	t_{exp} (min)	ΔS_{bp} (mm)	ΔP (mm)
1	A	4	14	2951	6.8	4.9	8.5	11.1	0.85	3.9
2	A	4	17	3410	8.0	4.2	9.9	13.6	1.11	5.1
3	A	4	20	3827	7.8	4.3	11.7	16.0	1.17	6.2
4	B	4	6	1502	6.0	2.8	3.9	3.4	0.46	1.4
5	B	4	12	2542	4.7	2.2	7.2	7.9	0.56	1.9
6	B	4	20	3627	7.3	1.9	10.8	14.4	1.08	4.9
7	C	5	9	2688	6.3	3.0	5.6	5.9	0.70	1.0
8	C	5	12	3293	5.5	2.2	7.2	8.1	0.72	1.6
9	C	5	15	3897	6.1	1.9	9.0	10.7	0.91	3.1
10	D	5	9	2698	7.7	4.4	5.8	5.5	0.85	1.3
11[a]	D	5	11	3148	5.9	3.8	7.0	7.3	0.75	1.4
12	D	5	13	3606	5.5	3.1	8.2	8.9	0.78	2.0
13[a]	E	6	8	2796	8.0	5.8	4.8	4.7	0.93	2.9
14	E	6	11	3513	4.6	4.2	6.6	6.8	0.63	2.5
15	E	6	14	4216	3.9	3.7	8.1	9.4	0.61	3.7
16	F	6	8	2573	5.1	2.7	4.6	5.0	0.58	1.9
17	F	6	11	3270	5.5	2.1	5.8	7.7	0.75	3.5
18[a]	F	6	15	4104	5.6	1.9	7.7	11.4	0.87	5.7

D_{bp} and D_{exp} are the defect values based on bioheat simulations for the bubble packing layout and the experimental layout, respectively; t_{bp} and t_{exp} are the simulated freezing durations for the bubble packing layout and the experimental layout, respectively; ΔS_{bp} is the average difference in freezing front location between bubble packing planning and the target region contour; and, ΔP is the average difference in the cryoprobe locations between bubble packing planning and the experimental layout.
The target region contours are displayed in Fig. 4.
[a] Presented in Fig. 5.

gion (this average difference is also referred to as uncertainty in the freezing front location). The uncertainty in freezing front location ranges from 0.5 mm to 1.2 mm, with an average value of 0.8 mm. Similar uncertainty calculations for the experimental locations of the cryoprobes yield much lower values (ranging from 0.2 mm to 0.7 mm, with an average value of 0.4 mm), since D_{exp} is smaller than D_{bp}. In the context of cryosurgery, where uncertainties associated with estimating the freezing front location via ultrasound imaging can easily exceed 1 mm [14], an average difference of 0.8 mm associated with planning is deemed acceptable. (For other sources of uncertainty in bioheat simulation, see Ref. [25]).

For the purpose of discussion, bubble packing results for three representative cases are shown in Fig. 5. Fig. 5a displays the results for Case 11, where a good match is found between the cryoprobe locations during experimentation and computerized planning using bubble packing. The average difference in cryoprobe locations between bubble packing results and the experimental locations, ΔP, is 1.4 mm. The defect values in this case are $D_{exp} = 3.8\%$ and $D_{bp} = 5.9\%$, which correspond to uncertainty in freezing front location of 0.49 mm and 0.75 mm, respectively.

Results for the above case were obtained using an average cryoprobe thermal history, as specified in the second paragraph of the current section. In a more detailed analysis of Case 11, where the actual thermal history for each cryoprobe is taken into account, an overall defect value of 1.5% is found. The increase in defect values from 1.5% to 3.8% is attributed to the application of a generic cryoprobe thermal history. Given the already low level of uncertainty in freezing front location, and the added computational cost associated with incorporating a specific thermal history for each cryoprobe, the application of a generic thermal history is deemed justified. This conclusion has further implications on computerized planning in general, where the actual thermal performance of a specific cryoprobe is difficult to establish *a priori*.

Fig. 5b displays results for Case 13, which has one of the highest defect values out of the 18 studied cases, which is 8.0%. It can be seen from Fig. 5b that most of that defect is found in the upper-right part of the target region, which is the result of the close proximity of the two cryoprobes in the relevant experimental setup (7.1 mm apart); the planning algorithm is not designed to place cryoprobes at such a close proximity. Nonetheless, even with this unique case, bubble packing still produces a result with an average freezing front uncertainty of 0.93 mm.

While experimental results in Case 13 were obtained using six cryoprobes, the quality of bubble packing was further investigated

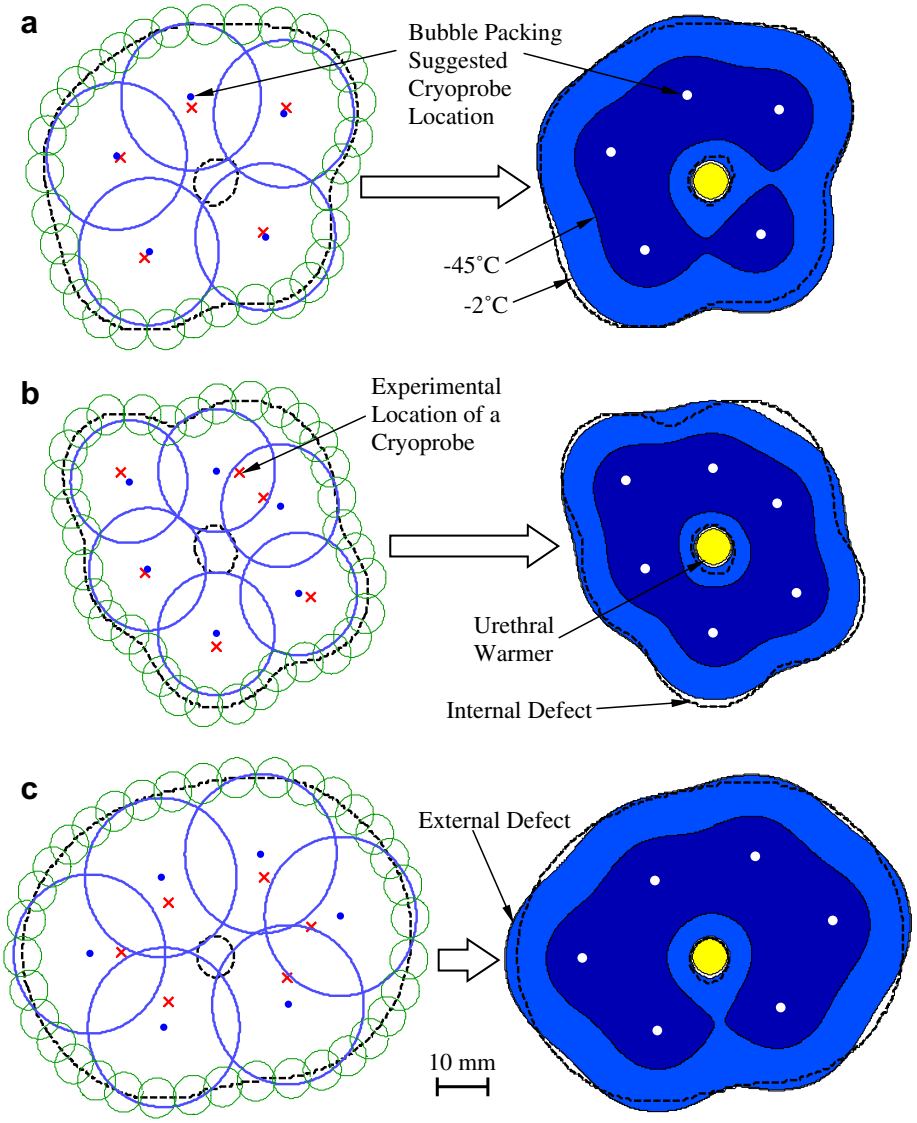

Fig. 5. Bubble packing results and the corresponding simulated temperature field for representative Cases: (a) 11, (b) 13, and (c) 18.

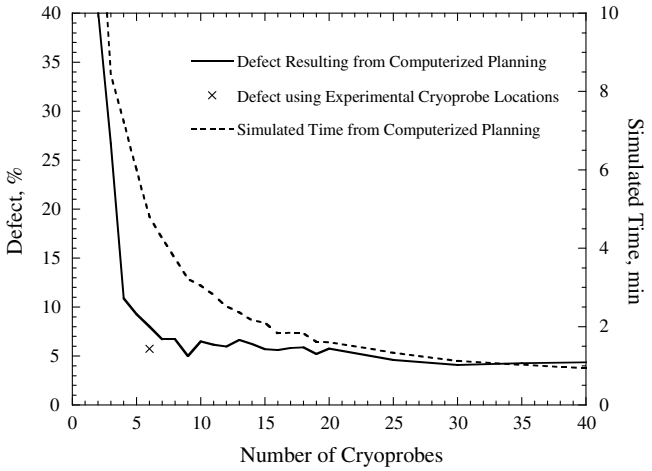

Fig. 6. The effect of the number of cryoprobes on the overall defect and the simulated time as a function of the number of cryoprobes, demonstrated on Case 13; the defect using the experimental cryoprobe layout is also shown.

with respect to the number of cryoprobes, to test the commonly made argument by cryodevice manufacturers that a larger number of cryoprobes is superior. Fig. 6 displays defect results for Case 13 as a function of the number of cryoprobes, up to an unrealistically high number of 40. As could be expected, using fewer than six cryoprobes leads to a dramatic increase in the defect area with the decreasing number of cryoprobes. With some minor perturbations, a trend of decreasing defect with the increasing number of cryoprobes is evident, with an overall improvement between six cryoprobes and 40 cryoprobes of about 4%. The benefit of such defect value improvement, at the expense of increased clinical complications and difficulties, makes the use of a larger number of cryoprobes undesirable. However, some improvement is sometimes observed when adding only a few cryoprobes (a 3% decrease in defect upon using nine cryoprobes in Case 13). Thus, computerized planning can potentially be used to determine an optimal number of cryoprobes, but the cost-effectiveness of an increased number of cryoprobes remains to be determined.

Another advantage in increasing the number of cryoprobes is the resulting increase in the cooling power of the system, which may decrease the clinical operation time. It can be seen from Fig. 6 that the simulated freezing runtime decays exponentially with time. For example, the freezing durations using 6, 8, and 10 cryoprobes are predicted to be 4.8, 3.7, and 3.2 min, respectively. Thus, one must also take into account the potential reduction in operation time when evaluating the cost-effectiveness of an increased number of cryoprobes.

Next, the effect of bubble packing on the duration of freezing is analyzed. While the simulated time for the actual cryoprobe layout, t_{exp}, may vary in comparison with the simulated time for bubble packing results, t_{bp}, when t_{exp} is shorter than t_{bp} (4 out of 18 cases), the average difference is only 0.3 min, with a maximum value of 0.5 min (Table 2). Conversely, for the cases in which t_{bp} is shorter than t_{exp}, the average difference is 1.8 min and the maximum difference is 4.3 min (14 out of 18 cases). While 0.5 min out of the duration of the freezing process may be considered insignificant in terms of clinical operation, 4.3 min is definitely significant.

This general trend of simulation-time reduction when using the bubble-packing technique can be explained by evaluating the results for a specific cryoprobe layout. For cryoprobe layout F (Cases 16 through 18), the difference in simulation-time is negligible for the first point in time—0.4 min for Case 16. The same difference increases to 1.9 min and 3.7 min in subsequent the cases, respectively. As shown in Table 2, the difference in simulation-time has a direct relationship to the average difference in the cryoprobe locations, ΔP. As the target region size increases from Case 16 to Case 18, the value for ΔP grows accordingly (1.9, 3.5, and 5.7 mm, respectively). As shown in Fig. 5c, the cryoprobe locations suggested by bubble packing for Case 18 are distributed similarly to the experimental locations, but placed closer to the external boundary. Thus, as the size of the frozen region grows, the cryoprobes resulting from bubble packing are also moved outwards. Bubble packing, in turn, provides a superior solution in terms of run time (3.7 min faster), but an inferior solution in terms of defect (5.6% compared to 1.9% for the experimental layout). Similar trends are seen in other layouts as well.

Finally, the discussion turns to the specific modifications made to bubble packing in the current study. When the original bubble-packing technique was applied to the 18 cases displayed in Fig. 4, an average defect of 14.6% was calculated (Fig. 3a for example), which corresponds to an uncertainty of 2.3 mm in the prediction of the freezing front location. When attractive forces were eliminated in the bubble packing algorithm, the average defect was reduced to 13.1% (Fig. 3b for example). When boundary bubbles were added, the average defect was further reduced to 6.1%. While further optimization of the technique is deemed unnecessary in the current study, bubble packing may be further optimized with respect to organ shape and size.

5. Summary and conclusions

Experimental validation of computerized planning via bubble packing has been presented in this study. In order to increase the quality of bubble packing planning, three modifications have been made to the original scheme: attractive forces were eliminated, the overlap ratio between bubbles was increased, and the radius of boundary bubbles was increased from an infinitesimal value to 4 mm. These modifications are related to the parameters most affecting the quality of planning; however, the scheme can further be optimized for increased quality.

Bubble packing planning was compared with experimental results from six different experimental layouts, at three points in time for each experiment, yielding a total of 18 cases. For each case, the target region for planning was defined as the reconstructed shape of the frozen region, taken from video recording of the experiment, using a reconstruction methodology published recently. Using the defect region concept, bioheat transfer simulations were used to evaluate the quality of the cryoprobe layout suggested by bubble packing, in comparison with the experimentally applied cryoprobe layout. Results indicate defect areas of less than 8% and an average value of 6.1%. This defect corresponds to an average mismatch of 0.8 mm between the freezing front and the contour of the target region, where the freezing front is the control variable used by clinicians for imaging-guided cryosurgery. For ultrasound imaging, where an uncertainty value of 1 mm is commonly accepted as a reasonable value for identification of the freezing front or a contour of an organ, prediction of the freezing front within a certainty of 0.8 mm is deemed adequate. Based on experimental results on gelatin, it is concluded that bubble packing planning is an efficient means to identify an optimal cryoprobe layout.

Results of this study support the previously made observation that—in contrast to a common argument made by cryodevice manufacturers—the quality of planning is not affected significantly by the number of cryoprobes beyond some threshold number. The overall freezing time however, is affected by the number of cryoprobes. When evaluating these observations, the additional trauma resulting from the increased number of cryoprobes must be taken into consideration, an effect which was not studied here.

Acknowledgements

This project is supported by the National Institute of Biomedical Imaging and Bioengineering (NIBIB) – NIH, Grant No. R01-EB003563-01,02,03,04. The authors would like to thank Mr. Jim Dillinger, Mr. John Fulmer, and Mr. Edward Wojciechowski, of the Machine Shop, Department of Mechanical Engineering, Carnegie Mellon University, Pittsburgh, PA, for assistance and advice in constructing the experimental system. The authors would also like to thank Dr. Ralph Miller of Allegheny General Hospital, Pittsburgh, Pennsylvania, for clinical advice.

References

[1] I.S. Cooper, A. Lee, Cryostatic congelation: a system for producing a limited controlled region of cooling or freezing of biological tissues, J. Nerve Ment. Dis. 133 (1961) 259–263.
[2] A.A. Gage, Cryosurgery in the treatment of cancer, Surg. Gynecol. Obstet. 174 (1992) 73–92.
[3] A.A. Gage, J. Baust, Mechanisms of tissue injury in cryosurgery, Cryobiology 37 (1998) 171–186.
[4] G.M. Onik, J.K. Cohen, G.D. Reyes, B. Rubinsky, Z.H. Chang, J. Baust, Transrectal ultrasound-guided percutaneous radical cryosurgical ablation of the prostate, Cancer 72 (4) (1993) 1291–1299.
[5] G.M. Onik, J.C. Gilbert, W. Hoddick, R. Filly, P. Callen, B. Rubinsky, L. Farrel, Sonographic monitoring of hepatic cryosurgery in an experimental animal model, Am. J. Roentgenol. 144 (5) (1985) 1043–1047.
[6] B. Rubinsky, J.C. Gilbert, G.M. Onik, M.S. Roos, S.T.S. Wong, K.M. Brennan, Monitoring cryosurgery in the brain and the prostate with proton NMR, Cryobiology 30 (1993) 191–199.
[7] T. Schulz, S. Puccini, J.P. Schneider, T. Kahn, Interventional and intra-operative MR: review and update of techniques and clinical experience, Eur. Radiol. 14 (12) (2004) 2212–2227.
[8] D.C. Lung, T.F. Stahovich, Y. Rabin, Computerized planning for multiprobe cryosurgery using a force-field analogy, Comp. Meth. Biomech. Biomed. Eng. 7 (2) (2004) 101–110.
[9] Y. Rabin, D.C. Lung, T.F. Stahovich, Computerized planning of cryosurgery using cryoprobes and cryoheaters, Technol. Cancer Res. T. 3 (3) (2004) 227–243.
[10] Y. Rabin, T.F. Stahovich, Cryoheater as a means of cryosurgery control, Phys. Med. Biol. 48 (2003) 619–632.
[11] M.R. Rossi, Y. Rabin, Experimental verification of numerical simulations of cryosurgery with application to computerized planning, Phys. Med. Biol. 52 (2007) 4553–4567.
[12] M.R. Rossi, Y. Rabin, Analysis of a numerical scheme for bioheat simulations of cryosurgery and its experimental validation on a phantom material, in: H.R. Arabnia (Ed.), Proceedings of the 2007 International Conference on Modeling, Simulation and Visualization Methods (Las Vegas, Nevada), CSREA Press, USA, 2007, pp. 187–193.
[13] M.R. Rossi, D. Tanaka, K. Shimada, Y. Rabin, An efficient numerical technique for bioheat simulations and its application to computerized cryosurgery planning, Comput. Meth. Prog. Bio. 85 (1) (2007) 41–50.
[14] D. Tanaka, M.R. Rossi, K. Shimada, Y. Rabin, Towards intra-operative computerized planning of prostate cryosurgery, Int. J. Med. Robot. Comp. 3 (2007) 10–19.
[15] D. Tanaka, K. Shimada, Y. Rabin, Two-phase computerized planning of cryosurgery using bubble packing and force-field analogy, J. Biomech. Eng.: Trans. ASME 128 (1) (2006) 49–58.
[16] D. Tanaka, K. Shimada, M.R. Rossi, Y. Rabin, Cryosurgery planning using bubble packing in 3D, Comp. Meth. Biomech. Biomed. Eng. 11 (2) (2008) 113–121.
[17] R. Baissalov, G.A. Sandison, B.J. Donnelly, J.C. Saliken, J.G. McKinnon, K. Muldrew, J.C. Rewcastle, A semi-empirical treatment planning model for optimization of multiprobe cryosurgery, Phys. Med. Biol. 45 (2000) 1085–1098.
[18] R. Baissalov, G.A. Sandison, D. Reynolds, K. Muldrew, Simultaneous optimization of cryoprobe placement and thermal protocol for cryosurgery, Phys. Med. Biol. 46 (2001) 1799–1814.
[19] R.G. Keanini, B. Rubinsky, Optimization of multiprobe cryosurgery, J. Heat Trans. ASME 114 (1992) 796–802.
[20] Y. Rabin, T.B. Julian, N. Wolmark, Method and apparatus for heating during cryosurgery, US Patent No. 5899897, 1999.
[21] K. Shimada, Physically-based mesh generation: automated triangulation of surfaces and volumes via bubble packing, Ph.D. Thesis, Massachusetts Institute of Technology, Cambridge, MA, 1993.
[22] Y. Rabin, A. Shitzer, Numerical solution of the multidimensional freezing problem during cryosurgery, J. Biomech. Eng. Trans. ASME 120 (1) (1998) 32–37.
[23] H.H. Pennes, Analysis of tissue and arterial blood temperatures in the resting human forearm, J. App. Phys. 1 (1948) 93–122.
[24] Y. Rabin, E. Korin, An efficient numerical solution for the multidimensional solidification (or melting) problem using a microcomputer, Int. J. Heat Mass Transfer 36 (3) (1993) 673–683.
[25] Y. Rabin, A general model for the propagation of uncertainty in measurements into heat transfer simulations and its application to cryobiology, Cryobiology 46 (2) (2003) 109–120.
[26] J.P. Holman, Heat Transfer, ninth ed., McGraw-Hill, New York, 2002.